Primljen / Received: 26.8.2023.
Ispravljen / Corrected: 10.3.2024.
Prihvaćen / Accepted: 18.5.2024.
Dostupno online / Available online: 10.7.2024.

Analysis of GFRP-reinforced beams in enhanced SCC

Authors:

Assist.Prof. **Prithiviraj Chidambaram**, PhD. CE
SRM Madurai College for Engineering and Technology
Department of Civil Engineering
Madurai, India
rajprithivi3@gmail.com
Corresponding author

Assoc.Prof. **Saravanan Jagadeesan**, PhD. CE
Annamalai University
Department of Civil and Structural Engineering
Chidambaram, India
ausjs5070@gmail.com

Research Paper

Prithiviraj Chidambaram, Saravanan Jagadeesan

Analysis of GFRP-reinforced beams in enhanced SCC

This study investigated the flexural behaviour of glass fibre-reinforced polymer (GFRP)-reinforced beams with two different ratios (0.68 % and 1.03 %) using traditional Self-Compacting Concrete (SCC) and SCC with 30 % Ultrafine Slag (UFS). The study analysed crack patterns, failure modes, load-deflection responses, strains in the concrete and reinforcement, and the influence of the reinforcement ratio and SCC compressive strength. The results indicated that under-reinforcement led to the rupture of the GFRP, balanced reinforcement resulted in bar and concrete failures, and over-reinforced beams mainly experienced compression zone concrete crushing. This study compared the ACI Flexural Design Guidelines (2015) with the experimental data.

Key words:
flexural behaviour, glass fibre reinforced polymer (GFRP), self-compacting concrete (SCC), ultrafine slag (UFS), flexural design guidelines

Prethodno priopćenje

Prithiviraj Chidambaram, Saravanan Jagadeesan

Analiza greda od samozbijajućeg betona ojačanih GFRP-om

U ovom istraživanju ispitano je ponašanje pri savijanju greda ojačanih staklenim vlaknima armiranim polimerom (eng. *Glass Fiber Reinforced Polymer* - GFRP) dvaju različitih omjera (0,68 % i 1,03 %) upotrebom tradicionalnog samozbijajućeg betona (eng. *Self-Compacting Concrete* - SCC) i SCC-a s 30 % ultrasitne troske (UFS). U istraživanju su analizirani uzorci pukotina, načini loma, odnosi opterećenje-progib, deformacije betona i armature te utjecaj omjera armature i tlačne čvrstoće SCC-a. Rezultati pokazuju da je premalo armature uzrokovalo pucanje polimera sa staklenim vlaknima, uravnotežena armatura dovela je do loma šipki i betona, a grede koje su sadržavale previše armature uglavnom su doživjele drobljenje betona u zoni stlačivanja. Ovo istraživanje usporedilo je ACI smjernice za projektiranje savijanja (2015.) s eksperimentalnim podacima.

Ključne riječi:
karakteristike savijanja, polimer ojačan staklenim vlaknima (GFRP), samozbijajući beton (SCC), ultrasitna troska (UFS), smjernice za projektiranje savijanja

1. Introduction

The construction industry has undergone significant advancements recently, particularly in concrete technology. With the growing demand for sustainable and eco-friendly construction practices, researchers are constantly exploring innovative materials and techniques to optimise the performance of concrete structures. One such development is the use of a glass fibre-reinforced polymer (GFRP) in combination with Ultrafine Slag (UFS) SCC for reinforced concrete (RC) beams subjected to flexural loads.

Steel bars are traditionally used for reinforcement in marine and coastal concrete structures; however, their susceptibility to corrosion in aggressive environments hampers durability. Alternative reinforcement materials and strategies should be explored to address this critical issue effectively [1-3]. The construction industry has gained significant attention to fibre-reinforced polymer (FRP) rebars, which offer exceptional corrosion resistance and are recommended in aggressive environments as a non-corrosive alternative to steel reinforcement, effectively addressing this issue [4]. Fibres are commonly manufactured from materials such as glass, basalt, carbon, and aramids. However, alternative fibres such as paper, wood, and asbestos have also been used in various studies [5-9]. Among these options, GFRP stands out as a favoured reinforcement in construction because of its resistance to corrosion, superior longitudinal tensile strength in the fibre direction, nonmagnetic properties, and lightweight properties [10-12]. In addition, the application of FRP bars in reinforcing marine infrastructure, particularly in environments prone to steel corrosion, leads to enhanced longevity and durability of marine structures. Consequently, the overall life cycle expenses are reduced [13, 14].

Similarly, SCC represents a notable advancement within the construction sector, finding extensive applications in diverse structural components such as beams, columns, and slabs [15-17]. This type of concrete is renowned for its remarkable ease of manipulation, exceptional ability to fill intricate spaces, and uniform consistency, rendering it a prime choice for complex geometries and densely packed reinforcement arrangements [18, 19]. The attainment of these desirable SCC properties necessitates a mix characterised by elevated powder content, reduced coarse aggregates, utilisation of a potent superplasticiser with high dispersing capabilities, and incorporation of a viscosity-modifying agent (VMA) [20, 21]. Among these constituents, the powder content is a pivotal factor that influences specific engineering attributes of SCC [22, 23]. Typically, SCC formulations require powder content ranging from 380 to 600 kg/m^3 [24, 25]. However, relying solely on cement to meet this powder content range is less desirable because of the associated higher carbon dioxide (CO_2) emissions stemming from increased cement volumes.

To address this concern, extensive research efforts have been made over the past three decades by various researchers [25-37, 38] to explore alternatives to cement, such as supplementary cementing materials (SCM) such as Fly Ash (FA), Ground Granulated Blast furnace Slag (GGBS), metakaolin (MK), Silica Fume (SF), Ultrafine Slag (UFS), and similar substances. These efforts have resulted in improved concrete performance in both the fresh and hardened states, reduced CO_2 emissions, and enhanced structural durability. A prominent recent advancement in durable construction involves the incorporation of UFS-based additives. UFS is a supplementary cementitious material that enhances the mechanical properties and durability of concrete [29, 39-45]. UFS consists of micronised particles with average sizes below 5 microns. UFS, sourced from granulated blast-furnace slag, is a byproduct of the iron and steel industry and is meticulously ground to obtain its ultrafine form. Research has shown that UFS can contribute to reduced porosity, improved particle packing, and enhanced bonds between the concrete matrix and reinforcement [17, 45-48]. The effect of UFS on the flexural behaviour of beams is an emerging area of investigation [16, 49, 50].

Numerous studies have investigated the flexural performance of concrete beams reinforced with Fibre-Reinforced Polymer (FRP) and conventional bars. Nanni [51] observed an increased flexural strength with sand-coated FRP bars, indicating the influence of the reinforcement and concrete properties on the strength. Benmokrane et al. [52] compared the cracking, load-bearing, and failure models between FRP and conventional bars, while GangaRao and Vijay [53] highlighted the factors affecting FRP-RC beam ductility. Xiao-jie et al. [54] found similarities in the long-term behaviour of SCC and Normal Vibrated Concrete (NVC) beams, noting a reduced deflection due to the lower modulus of elasticity in SCC. Kalpana and Subramanian [55] examined GFRP-RC beams with different concrete grades and bar sizes, revealing superior performance with higher-grade concrete. You et al. [56] studied low-reinforcement SCC beam flexure and compared hybrid and steel fibre RC beams, while Roja et al. [6] compared GFRP and TMT bars, demonstrating the limitations of GFRP. Mazaheripour et al. [57] introduced hybrid prestressed GFRP steel and SCC beams to improve deformability. Nikbin et al. [58] explored SCC fractures and ductility using mineral powders. Goldston et al. [13] investigated GFRP-reinforced high-strength concrete beams and observed different behaviours in under-reinforced and over-reinforced beams. Balachandu Koya and Sureshkumar [59] studied the flexural behaviour of high-strength SCC steel/GFRP beams and found comparable performance. Mithra et al. [60] explored SCC with GGBS and found optimal mixes with improved flexural behaviour. Patel and Balakrishna [61] investigated GGBS cement and slag sand-fine aggregate substitutions and identified the optimal replacements. Marshaline et al. [62] analysed reinforced SCC beams with improved fresh and hardened properties. Manju et al. [63] replaced fly ash in SCC beams and observed differences in performance. Vivek et al. [64] studied SCC with mineral admixtures of MK + GGBS and SF + GGBS, which showed enhanced flexural strength. Shijumon and Nalanth [65] investigated NVC and SCC beams with recycled concrete waste aggregates and SF additives to improve their properties and reduce shear cracking.

Researchers have investigated factors such as the reinforcement type, concrete properties, and additives. The findings include increased strength with sand-coated FRP bars, similarities in behaviour between SCC and NVC beams, and improved performance with higher-grade concrete and hybrid prestressed GFRP-steel SCC beams. Studies have also examined the effects of mineral powders, admixtures, and substitutions on flexural behaviour. Some studies have focused on enhancing the fresh and hardened properties of reinforced SCC beams, while others have explored the impact of additives on shear cracking and overall properties. However, no studies have been conducted on the flexural performance of beams that integrate a blend of GFRP reinforcement, SCC, and UFS. In this study, an effort was made to discuss the flexural behaviour of beams reinforced with GFRP instead of steel. The beams were constructed using both traditional SCC and SCC containing 30 % UFS. The experimental test outcomes and ACI recommendations for the FRP-RC beam design were compared.

2. Experimental program

2.1. Constituent materials and mix proportions

As per the IS 12269-2013 guidelines [66], Ordinary Portland Cement (OPC) 53 grade, sourced from Ultra-Tech Pvt. Ltd., was utilised [66]. In place of OPC, UFS is commercially recognised as Alccofine 1203, which was produced by Counto Micro Fine Products Pvt. Ltd., Goa. Table 1 lists the chemical characteristics of the cement and ultrafine slag sourced from the supplier.

Table 1. Chemical properties of OPC and UFS

Chemical composition [%]		
Component	**Cement**	**Ultrafine slag**
CaO	66.67	32.20
SiO_2	18.91	35.30
Fe_2O_3	4.94	1.20
Al_2O_3	4.51	21.40
SO_3	2.5	0.13
MgO	0.87	6.20
K_2O	0.43	-
Na_2O	0.12	-

Figure 1 shows the results of scanning electron microscopy (SEM) at 1000x magnification and Energy Dispersive Spectroscopy (EDS) analyses of the OPC 53-grade cement and UFS particles. Examination revealed that the cement particles exhibited irregular shapes, whereas the UFS particles were irregularly shaped but featured sharp edges. Locally sourced river sand meets zone III specifications as a fine aggregate, whereas crushed angular coarse aggregate conforming to IS 383-1970 [67] is used. Table 2 lists the material properties, and Figure 2 shows the aggregate particle size distribution. To adhere to IS: 9103-2018 [68], a BASF Master Glenium Sky 8233 superplasticiser (polycarboxylic ether) was employed [68]. The investigation exclusively used regular tap water. Prior research has assessed the key attributes of the constituent components and their characteristics in both fresh and solidified states

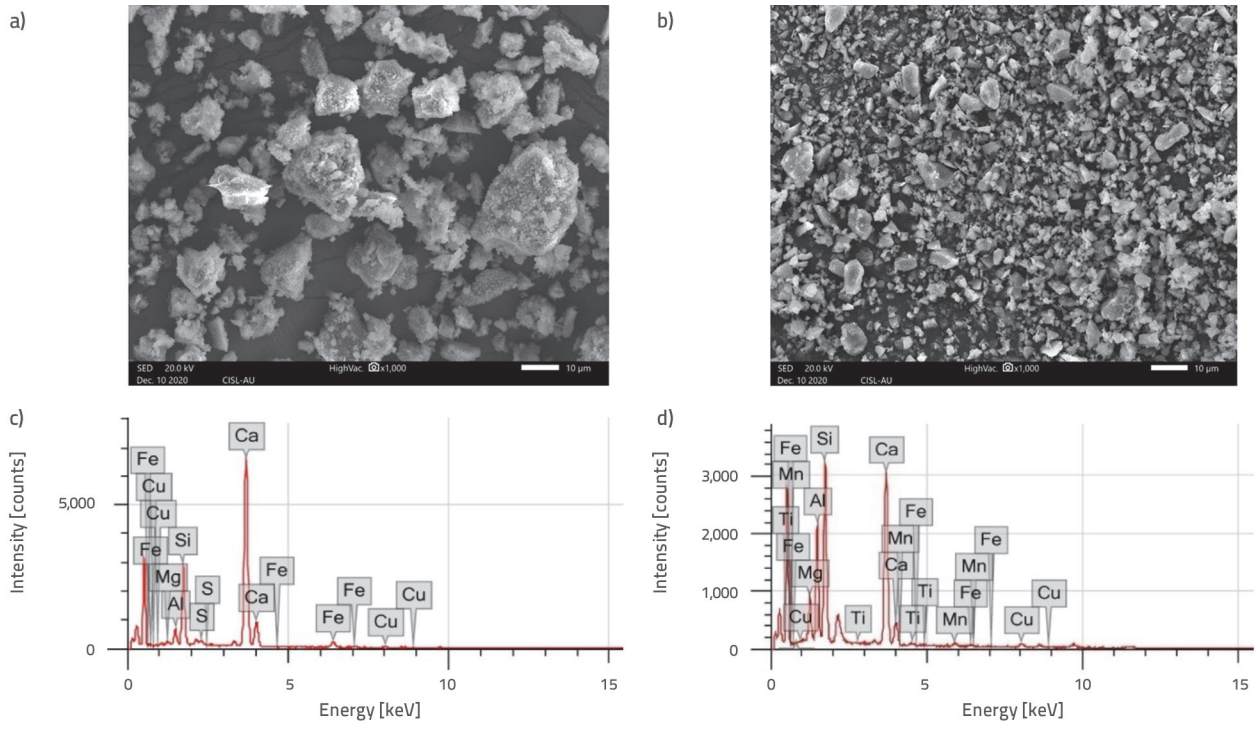

Figure 1. a) and b) SEM; c) and d) EDS outputs of OPC and UFS

Table 2. Physical Properties of constituent materials

Description	Size	Specific gravity	Water absorption	Fines modulus	Specific surface area
Cement	90 μ	3.15	–	–	225 m^2/kg
UFS	4 to 6 μ	2.86	–	–	1200 m^2/kg
Fine aggregate	< 4.75 mm	2.68	0.42	2.88	–
Coarse aggregate	20 mm – 4.75 mm	2.7	0.92	7.08	–

[20, 44, 46]. The fresh properties of the SCC were evaluated according to ISO 1920-13:2018 [25], including slump flow, V-funnel, and L-box tests. These tests provide essential insights for assessing the flow, filling, and passing abilities of SCC. Table 3 outlines the materials necessary for the SCC beams that were used for measurements and casting. In addition, it exhibited fresh properties and compressive strength.

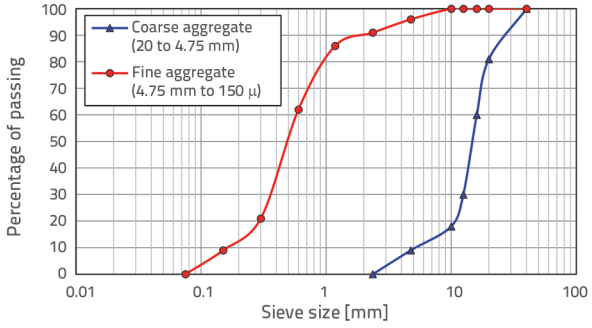

Figure 2. Particle size distribution of aggregates

Table 3. Mix proportions and Properties of SCC

Description	SCCA0	SCCA30
Cement [kg/m^3]	465	325.5
UFS [kg/m^3]	0	139.5
Fine aggregate [kg/m^3]	915	915
Coarse aggregate [kg/m^3]	836	836
Water [kg/m^3]	186	186
Superplasticiser [kg/m^3]	4.65	4.65
Slump flow [mm]	610	690
T50 [s]	5	4
V-Funnel [s]	6	3
L-Box ratio	0.81	0.95
Compressive strength [N/mm^2]	30.69	48.13

2.2. Reinforcement

Sand-coated GFRP obtained from Meena Fibres, Pondicherry, was employed as a reinforcing rod, as shown in Figure 3.a. The diameter of the tension and compression reinforcements was 12 mm, while the stirrups had a diameter of 8 mm with closed rings without flaps. Stirrups were uniformly placed along the beam to maintain consistency and isolate the variables. Varying the spacing could influence the structural behaviour, as the study focused on the flexural behaviour. Specimens consisting of three rebars of each diameter were tested and evaluated following the prescribed standards ASTM D7205/D7205M [69], as illustrated in Figures 3.b, 3.c and 3.d. The details of the anchorage are shown in Figure 3.e.

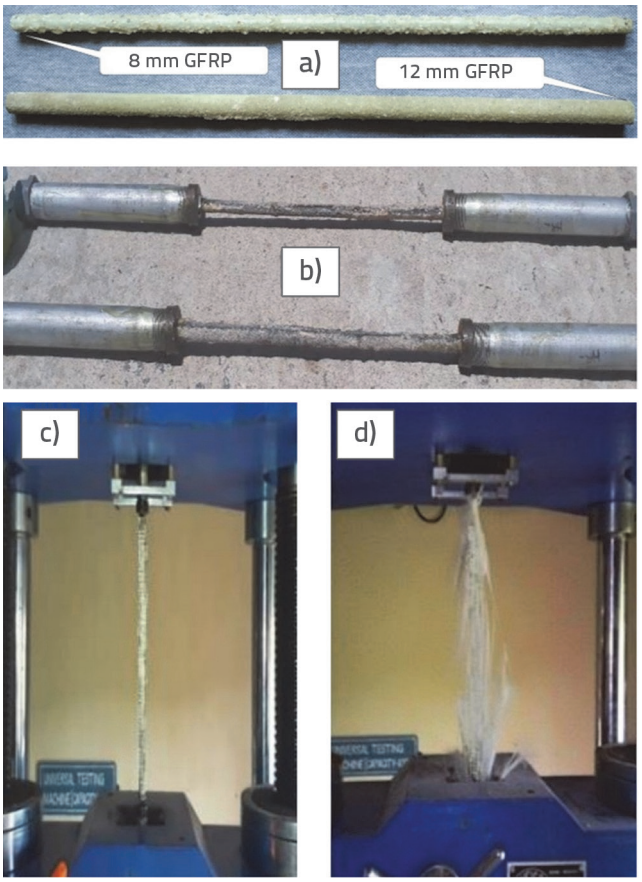

Figure 3. a) Sand-coated GFRP bars; b) GFRP bars with anchorage; c) Test setup, d) failure

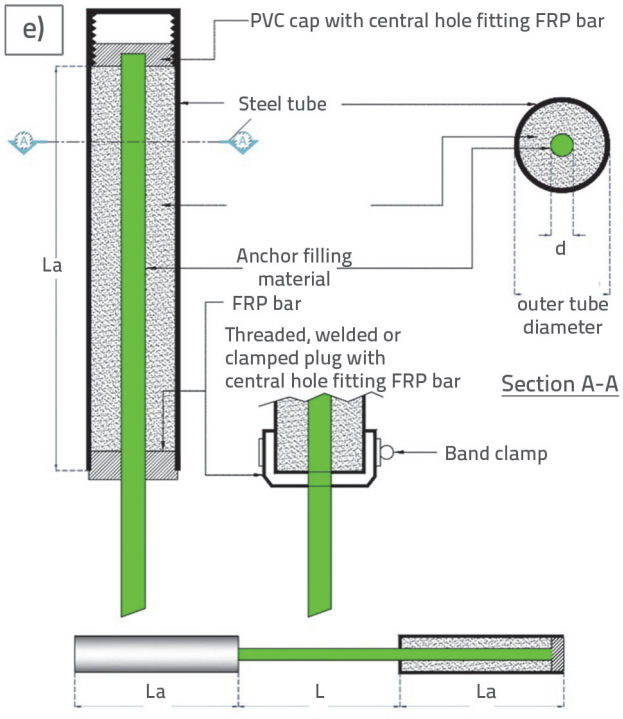

Figure 3. e) Anchorage details

The mechanical characteristics of the reinforcements are listed in Table 4. The average stress-strain diagrams for the analysed reinforcement bars are depicted in Figure 4, including a stress-strain curve specifically for the steel rebar provided for comparison.

Table 4. Mechanical properties of GFRP rebars

Diameter of rebar [mm]	Tensile strength [MPa]	Elastic modulus [GPa]
8	420.00	46.36
8	419.00	46.34
8	421.00	46.37
Mean	**420.00**	**46.36**
12	680.00	54.87
12	681.00	54.91
12	680.00	54.85
Mean	**680.33**	**54.88**

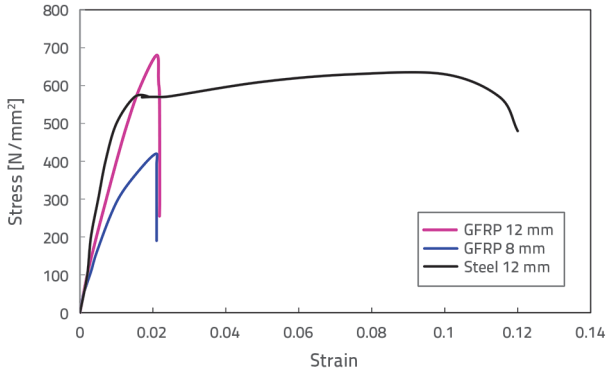

Figure 4. Stress-Strain curve of GFRP bars

2.3. Preparation of beams

Twelve full-scale beams were manufactured and subjected to static loading at two points, according to the ACI standard [70]. These beams had a length of 3000 mm and cross-sectional dimensions of 150 mm in width and 250 mm (depth). There was a 25 mm concrete cover from the outer edge of the stirrups along all sides of the beams. The configuration of the cross-section is shown in Figure 5.

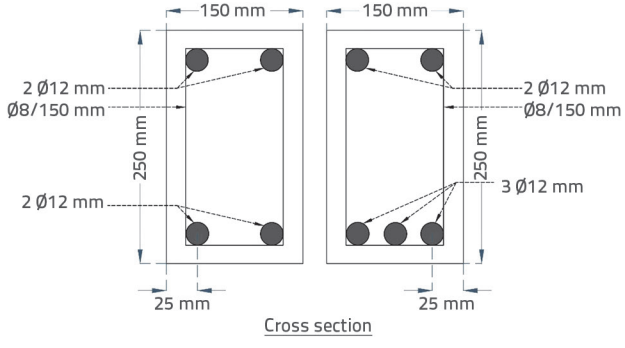

Figure 5.Cross-section of SCC beams

The beams were divided into four groups based on their mixture compositions and reinforcement proportions. Each of the four groups consisted of three beams. Specifically, Group I and II beams were constructed using the SCCA0 mixture, whereas Group III and IV beams employed the SCCA30 mixture. Group I and III beams share a reinforcement ratio (ρ_f) of 0.68 %, whereas Group II and IV beams possess a reinforcement ratio of 1.03 %. The beams are labelled A–B–C, where A indicates the Alccofine (UFS) proportion, B signifies the reinforcement ratio, and C represents the number of beam specimens. To illustrate, beam A30-G1-B1 was crafted with 30 % UFS content (A30) and a 0.68 % GFRP tension reinforcement ratio (G1) and denoted as specimen B1. Table 5 provides a comprehensive overview of the beam details.

2.4. Test setup and procedure

All beams were subjected to a 28-day site curing period after casting, during which wet gunny bags were used to maintain consistent moisture levels, and were protected from extreme temperature variations to ensure proper hydration and strength development. The beams were subjected to a simple support configuration and were loaded with two monotonically concentrated beams. The effective span of the beams was

Table 5. Summary of beam details

Mix	Group	Beam ID	Compression reinforcement	Tension reinforcement	ρ_f [%]	Condition of reinforcement
SCCA0	I	A0-G1-B1	2Ø12	2Ø12	0.68	Under-reinforcement
		A0-G1-B2	2Ø12	2Ø12		
		A0-G1-B3	2Ø12	2Ø12		
	II	A0-G2-B1	2Ø12	3Ø12	1.03	Over-reinforcement
		A0-G2-B2	2Ø12	3Ø12		
		A0-G2-B3	2Ø12	3Ø12		
SCCA30	III	A30-G1-B1	2Ø12	2Ø12	0.68	Under-reinforcement
		A30-G1-B2	2Ø12	2Ø12		
		A30-G1-B3	2Ø12	2Ø12		
	IV	A30-G2-B1	2Ø12	3Ø12	1.03	Balanced-reinforcement
		A30-G2-B2	2Ø12	3Ø12		
		A30-G2-B3	2Ø12	3Ø12		

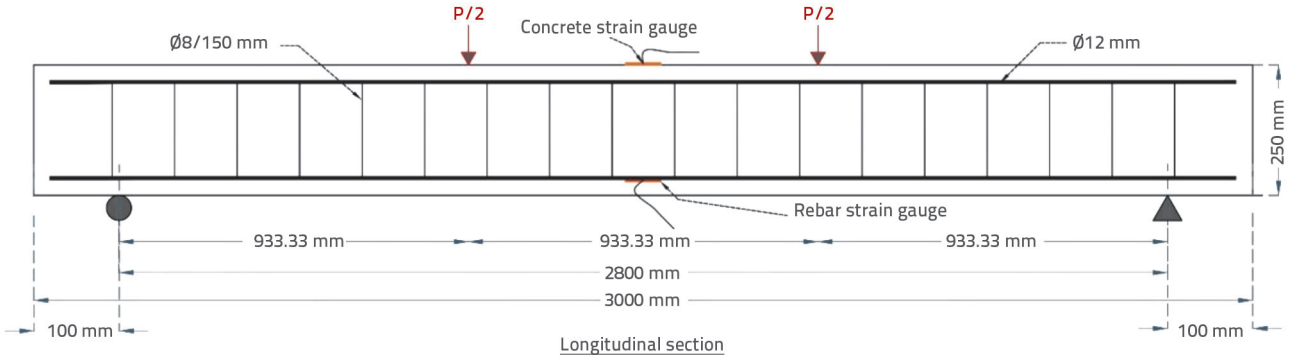

Figure 6. Schematic diagram of longitudinal cross-section with loading

2800 mm, featuring a shear span of 933.33 mm (L/3) and 100 mm overhangs on both sides, as illustrated in Figure 6. The beams were anchored at their ends using a hinge and roller, thereby enabling deflection under a gradually increasing load. A hydraulic jack with a capacity of 500 kN was employed for the load. This load was incrementally increased at 2.5 kN intervals, utilising a steel spreader (I-section) to transfer the load to the beam specimen. The load was meticulously monitored using a proving ring. To assess the strain during loading, two 5 mm gauge length surface strain gauges were affixed on each side of all beams, along with two strain gauges positioned in the centre of the GFRP reinforcement, connected to a strain indicator. The mid-span deflection was measured using dial gauges with a minimum count of 0.01. Throughout the loading process, various observations were made, including deflections, concrete surface strains, rebar strains, and beam face cracks, which were recorded diligently at each load increment. The experimental setup is shown in Figure 7.

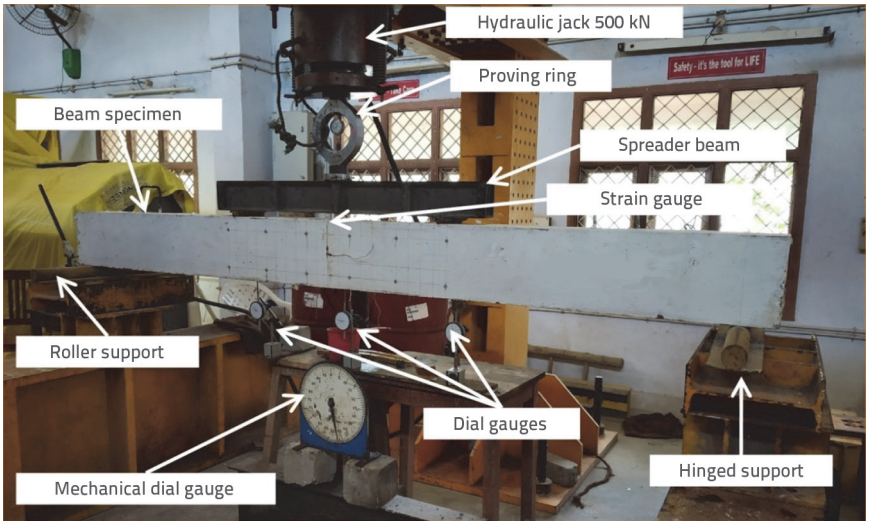

Figure 7. Experimental test setup

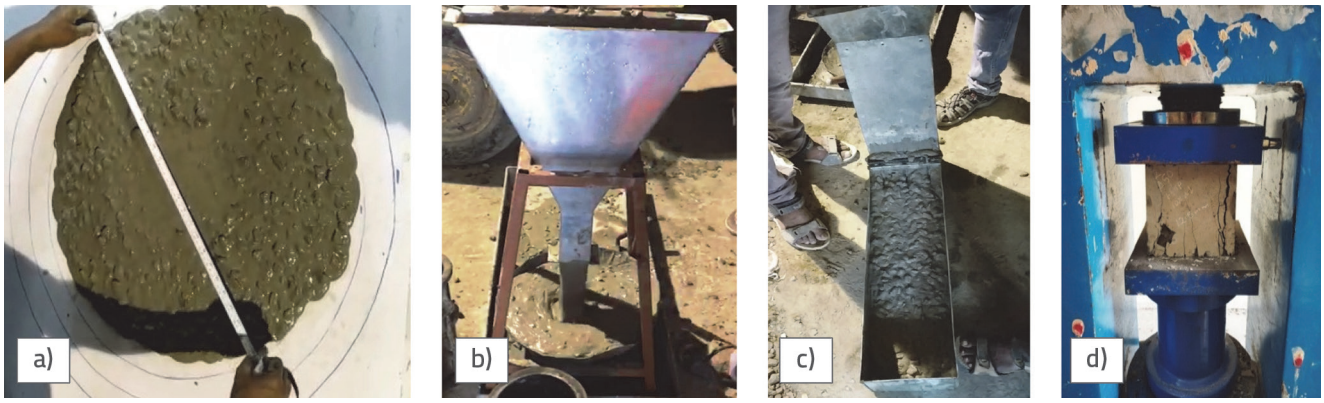

Figure 8. Testing of fresh and hardened state of SCC: a) Slump flow; b) V-Funnel; c) L-Box; d) Compressive strength

3. Result and discussion

3.1. Fresh and hardened properties of SCC

The investigation into the SCC properties revealed significant enhancements with the addition of ultrafine slag. Based on prior research [20, 44, 46], the UFS-optimised mixtures exhibited improved flowability, filling ability, passing ability, and compressive strength, particularly at 30 % inclusion. The limited research on SCC with UFS highlights the novelty of this study, in which 30 % of UFS utilisation represents a significant advancement. Despite the initial cost concerns, UFS offers long-term viability and sustainability benefits, justifying its integration into SCC formulations. The UFS improved particle packing, reduced segregation, and enhanced fresh properties, while its pozzolanic reactivity significantly boosted the compressive strength, demonstrating its effectiveness as a supplementary cementitious material. The examination of SCC properties is complemented by Figure 8, which illustrates key laboratory experimental results, such as slump flow, V-funnel, L-box, and compressive strength tests. This comprehensive understanding of SCC properties and performance led to an examination of SCC beam analyses with and without UFS, which is discussed in the following section.

3.2 Cracking behaviour of SCC beams

Table 6 presents the outcomes of the experimental trials involving SCC beams. Before being subjected to loads, the beams maintained their rigidity and were devoid of cracks. With the gradual application of external forces, the beams underwent deformation, leading to crack initiation within the tension zone.

Table 6. Experimental test results of SCC beams

Beam ID	Load [kN]		Deflection [mm]		Ultimate strain		Crack width [mm]	Mode of Failure
	First crack	Ultimate	First crack	Ultimate	Concrete	Rebar		
A0-G1-B1	12.5	59.34	1.1	32.87	0.00173	0.0148	0.6	FRP rupture
A0-G1-B2	12.5	59.21	1.8	31.73	0.00211	0.0179	0.58	
A0-G1-B3	15	60.13	1.99	32.68	0.00195	0.0173	0.62	
Mean	**13.33**	**59.56**	**1.63**	**32.43**	**0.00193**	**0.0167**	**0.60**	
A0-G2-B1	12.5	70.13	1.11	33.83	0.00317	0.0148	0.54	Concrete crushing
A0-G2-B2	12.5	71.2	1.78	29	0.00323	0.0133	0.55	
A0-G2-B3	10	67.5	1.11	31.72	0.00301	0.0137	0.52	
Mean	**11.67**	**69.61**	**1.33**	**31.52**	**0.0031**	**0.0139**	**0.54**	
A30-G1-B1	17.5	61.11	9	33.24	0.00228	0.0171	0.63	FRP rupture
A30-G1-B2	15	60.62	8.75	33.32	0.00223	0.0166	0.62	
A30-G1-B3	17.5	62.7	10.66	33.76	0.00231	0.0162	0.67	
Mean	**16.67**	**61.48**	**9.47**	**33.44**	**0.0023**	**0.0166**	**0.64**	
A30-G2-B1	17.5	57.5	4.8	30.2	0.00332	0.01577	0.6	FRP rupture and Concrete crushing
A30-G2-B2	17.5	77.35	4.97	34	0.0032	0.01634	0.68	
A30-G2-B3	17.5	70	3.09	35.19	0.00316	0.01721	0.63	
Mean	**17.50**	**73.69**	**4.29**	**33.13**	**0.0032**	**0.0164**	**0.64**	

During the initial stages, smaller cracks became noticeable in the region with a consistent moment. As the load progressed, new cracks emerged, and pre-existing cracks expanded further. As the load continued to exert pressure on the beam, the cracks located away from the flexural zone assumed an inclined trajectory and progressively extended towards the loading point situated within the compression zone of the beam. The crack patterns commonly observed in SCC beams are shown in Figure 9.

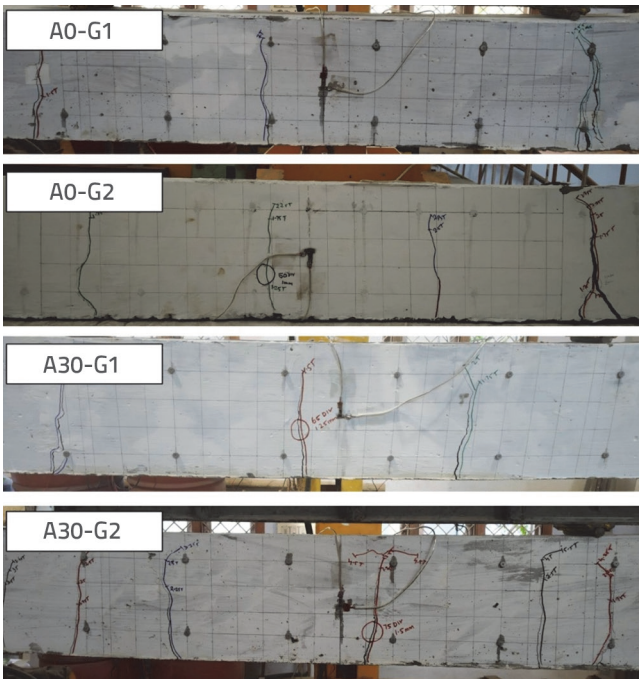

Figure 9. Typical crack patterns of SCC beams

The beams were categorised into four sets: Groups I and III (under-reinforced, where $\rho_f < \rho_{fb}$), and Groups II and IV (over-reinforced, where $\rho_f > \rho_{fb}$ and balanced, with $\rho_{fb} \leq \rho_f \leq 1.4$ respectively). The beams in Groups I and III (labelled A0-G1 and A30-G1) exhibited a similar pattern of cracking, characterised by fewer cracks, wider spaces between the cracks, and larger crack widths. This outcome can be linked to the lower reinforcement ratio (ρ_f= 0.68 %). As stated by (Kalpana and Subramanian 2011), [55] larger crack widths in GFRP-reinforced beams are acceptable because of the corrosion-resistant nature of GFRP. Group II beams (A0-G2), featuring a reinforcement ratio of ρ_f= 1.08 %, displayed a crack pattern similar to Group I, but with a greater number of cracks, narrower spacing between cracks, and smaller crack widths. This indicated a higher load-bearing capacity. Similarly, Group IV beams (A30-G2), also with a reinforcement ratio of ρ_f= 1.08 %, exhibited wider cracks with minimal spacing. Premature cracking occurred in all the beams because of the lower Young's modulus of the GFRP. This low modulus hampers its capacity to withstand deformations and efficiently distribute loads, thereby increasing the likelihood of premature cracking.

3.3. Failure mode of SCC beams

Failure of SCC-reinforced beams in Groups I and III occurred at the point of maximum bending moment. This failure occurs when the GFRP reinforcement ruptures, as shown in Figure 10.a. There were no prior indications of failure in these beams; instead, the failure was sudden and brittle. This type of failure has also been documented in the literature by Adam et al. (2015), Ashour and Habeeb (2008), and Goldston et al. (2017) [13, 71, 72]. In these cases, tension failure was observed in the FRP-reinforcing bars, whereas the upper concrete surface remained intact at the failure location. The failure patterns of the balanced reinforced beams in Group IV are shown in Figure 10.c. This failure occurred due to the rupture of the GFRP bar, followed by the crushing of the concrete. Meanwhile, the over-reinforced beams in Group II exhibited a distinct failure mode, as shown in Figure 10.b. In this case, vertical cracks emerged around the midspan of the over-reinforced GFRP beam and then propagated towards the support regions. As the load increased, flexure–shear cracks appeared closer to the supports. Ultimately, the failure of these beams resulted from compression failure of the concrete on the upper surface.

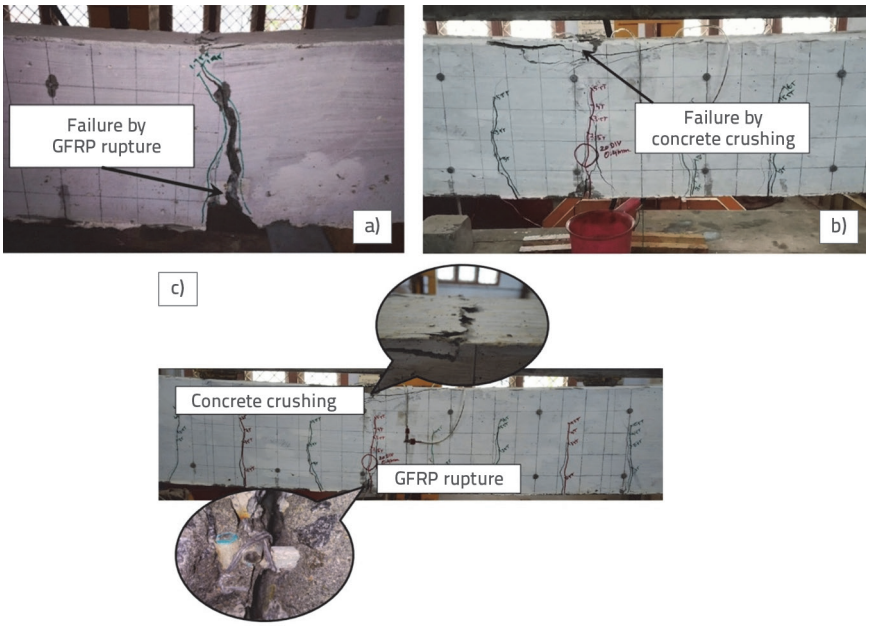

Figure 10. Typical failure mode of SCC beams: a) Under-reinforcement; b) Over-reinforcement; c) Balanced-reinforcement

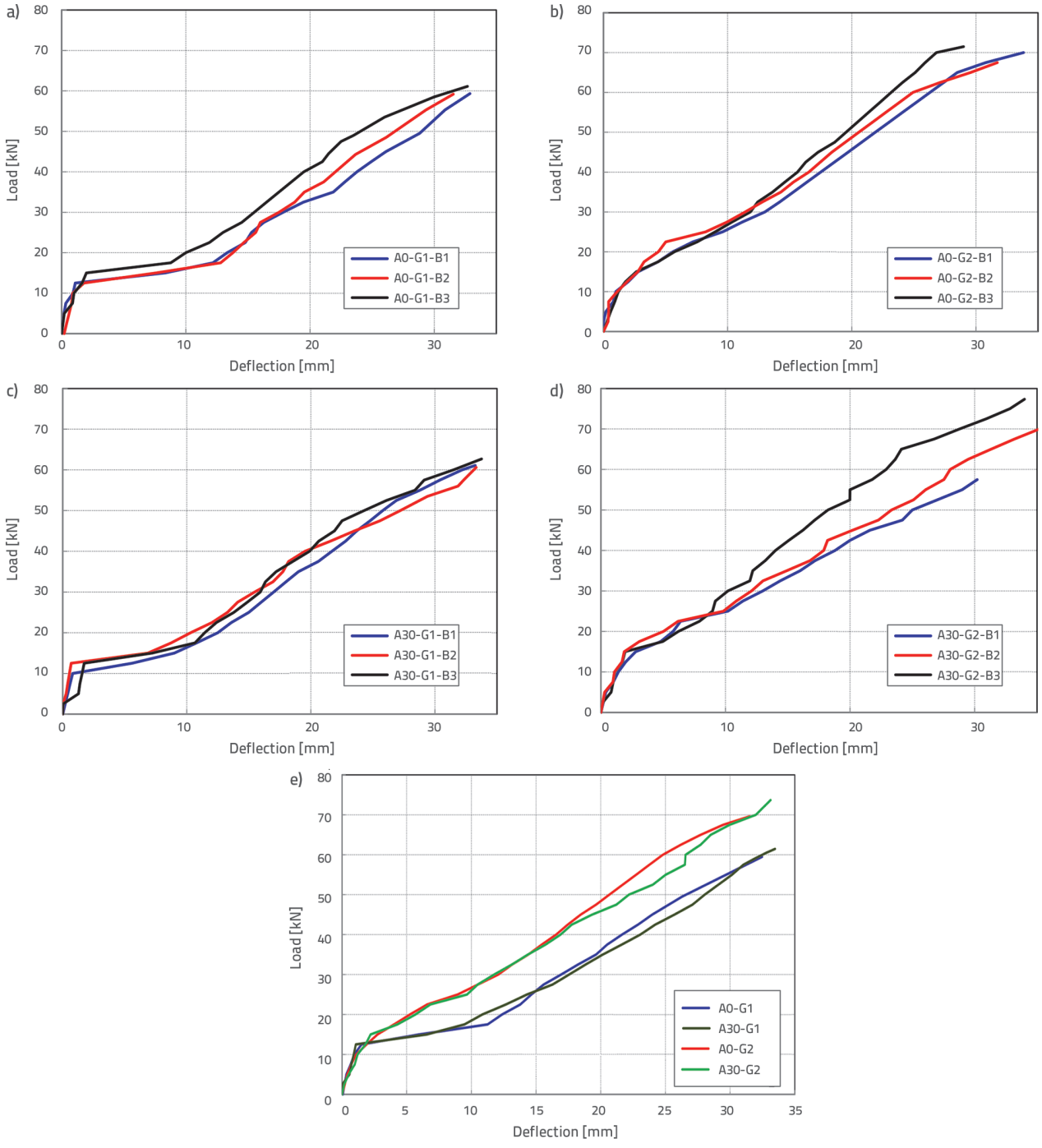

Figure 11. Load-deflection curves: a) A0-G1; b) A0-G2; c) A30-G1; d) A30-G2; e) average

3.4. Load deflection behaviour

Figure 11 shows the experimental load-deflection patterns of the beams. The load-deflection profiles of FRP-RC beams can be roughly segmented into two linear phases, indicating abrupt changes in the slope within the curve. The initial point, which is referred to as the first cracking point, marks the emergence of the first flexural crack in the beam. Following the onset of flexural cracking, the beams experienced a reduction in the slope. Due to the non-yielding nature of the FRP reinforcement, the load-deflection curve also maintains an almost linear trajectory towards failure from the point of cracking initiation. Consequently, these load-deflection curves displayed multiple minor fluctuations, signifying that the load capacity experienced sudden, slight drops during the loading process. These fluctuations caused the load-deflection curves to exhibit minor zigzag patterns instead of a straight linear progression. The occurrence of fibre slippage within the matrix was responsible for these fluctuations.

3.5. Strain behaviour in concrete and reinforcement

Figure 12 illustrates the load-strain behaviour of both the rebars and concrete, with the (XY) and (–XY) coordinates indicating the strain in the reinforcement and concrete, respectively. The concrete strain at failure is typically within the range of 0.0019–0.0035, as outlined in the American and Canadian standards [70, 73]. By contrast, GFRP typically experiences strains at failure between 0.013 and 0.017, according to Canadian standards [74]. No significant strain was observed in either the concrete or reinforcement due to deformation until the first crack was formed, after which there was a rapid increase in the strain values. A nearly linear section of the load-strain curves was observed for both the GFRP and concrete until failure. The relationship between the strain in the reinforcement and concrete and the failure mode is significant. For under-reinforced beams, the reinforcement strain approaches the ultimate strain, whereas the concrete strain does not, indicating a tension-failure mode. Lower concrete strain values represent rupture failure, where the assumed strain values are not attained because the concrete effectively resists tensile forces up to the formation of the first crack. The increase in loading leads to the propagation of cracks and allows the reinforcement to withstand tensile forces, resulting in an ultimate strain on the reinforcement. In the case of the balanced reinforced beam, the strains in the reinforcement and concrete were close to the ultimate strain, indicating balanced failure. For an over-reinforced beam, the strain in the concrete almost reached the ultimate strain but not in the reinforcement, indicating a compression failure mode.

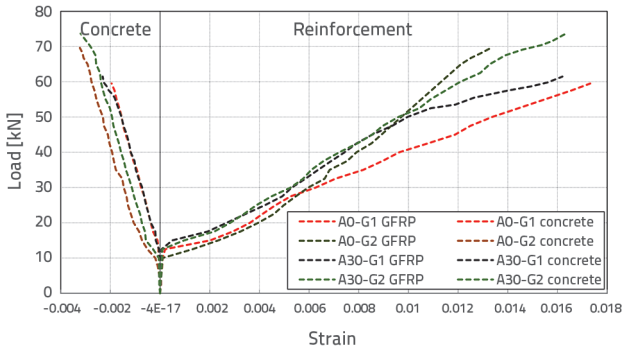

Figure12. Strain behaviour of SCC beams

3.6. Influence of reinforcement ratio

An increase in the proportion of tensile reinforcement improved the performance of the beams subjected to static loading. Augmented tensile reinforcement is also crucial for increasing the load-bearing capability and diminishing the deflection in simply supported beams, as stated in [71, 72]. This notion also supports empirical findings, which revealed that augmenting the quantity of tensile reinforcement resulted in an amplified load-bearing capacity and reduced midspan deflection. For instance, in conventional SCC beams, by increasing the reinforcement ratio from 0.68 % (A0-G1) to 1.03 % (A0-G2), there was a 20.33 % increase in the load-carrying capacity and a 9.83 % decrease in the midspan deflection. Similarly, in the UFS-based SCC beams, increasing the reinforcement ratio from 0.68 % (A30-G1) to 1.03 % (A30-G2) led to an 11.55 % improvement in the load-carrying capacity, accompanied by a 7.63 % increase in the midspan deflection.

3.7. Influence of concrete strength

The impact of concrete strength on all the examined parameters is limited in the case of both conventional and UFS-based Self-Compacting Concrete (SCC) beams with a reinforcement ratio (ρ_f) of 0.68 %. For beams designated as A0-G1 and A30-G1, the load-bearing capacity increased from 58.83 kN to 68.9 kN, marking a rise of approximately 15.7 %, as the conventional concrete strength of 30.69 N/mm^2 was replaced by the UFS-based concrete strength of 48.15 N/mm^2. However, the increase in the load-bearing capacity was restrained because the beams were under-reinforced, which caused the failure to be determined by the tensile strength of the reinforcement. The midspan deflection decreases by 1.57 %, transitioning from 32 mm (A0-G1) to 31.5 mm (A30-G1). In contrast, the behaviour of the over-reinforced beams was more influenced by the concrete strength, as elaborated in Goldston et al.'s study in 2017 [13], because the failure in this case was governed by the concrete strength itself. This investigation encompassed GFRP beams with a reinforcement ratio (ρ_f) of 1.03 %, categorised into over-reinforced (A0-G2) and balanced-reinforced (A30-G2) conditions. This change in reinforcement configuration was instigated by the increase in concrete strength from 30.69 N/mm^2 to 48.15 N/mm^2. Consequently, the augmented load-carrying capacity experienced a relatively modest increment of 7.8 % (from 71.5 kN to 77.35 kN), coupled with a 15.87 % upsurge in midspan deflection (from 29 mm to 34 mm).

3.8. Comparison of experimental results with standard recommendation

The experimental test results were compared with the FRP design recommendations provided by the ACI [69]. As outlined in these guidelines, the preferred mode of failure for FRP-RC beams is concrete crushing. This preference is due to the fact that FRP-RC beams exhibit a certain degree of "ductility" and plastic behaviour before reaching failure, a concept emphasised in the ACI guidelines [69]. Unlike conventional steel-RC beams, where the yielding of steel is relied upon to enhance ductility and act as an indicator of failure, FRP-RC beams follow a distinct design philosophy. Sudden failure caused by the rupture of FRP bars, a characteristic of linear-elastic FRP materials, is considered highly detrimental and should be avoided [51, 75, 76]. To mitigate the risk of such abrupt failures, the design of FRP-RC structures is oriented towards promoting failure

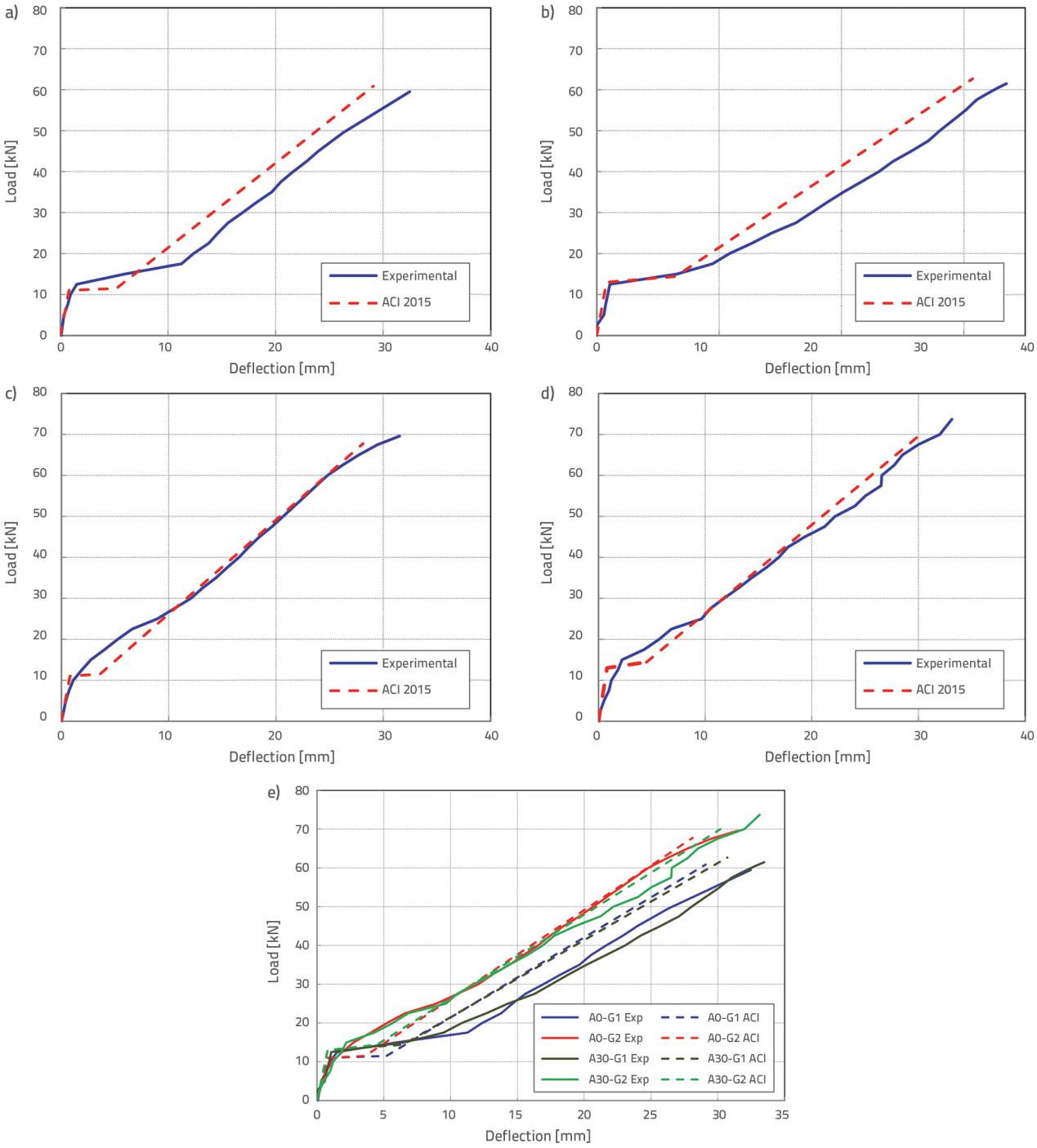

Figure 13. Comparison of Load-deflection curves of Experimental versus: a) A0-G1; b) A0-G2; c) A30-G; d) A30-G2; e) all average exp and ACI beams

through concrete crushing. This approach offers a type of pseudo-ductile failure that provides advanced warnings prior to structural collapse [4]. For the computation of the nominal flexural capacity (designed for flexure) and midspan deflection of FRP-RC beams, the guidelines presented in Table 8 provide the relevant FRP design code instructions [70]. Table 7 shows a comparison between the outcomes of the experiments and the forecasts made by the ACI [70]. This comparison gauged the percentage disparity between the two sets of results. Positive figures indicate instances where the design codes underestimated the performance, whereas negative values suggest cases where the design codes overestimated the performance. ACI [70] accurately anticipated the failure modes of GFRP-reinforced SCC beams. For beams with a reinforcement

ratio of 1.07, failure occurred because of the simultaneous crushing of both the GFRP bars and concrete. Meanwhile, Beams A0-G1 and A30-G1, featuring reinforcement ratios of 0.95 and 0.71, respectively, failed solely because of GFRP bar rupture. Conversely, beam A0-G2, with a reinforcement ratio of 1.42 (exceeding 1.4), experienced failure due to compression-side concrete crushing. Figure 13 illustrates a comparison between the load and deflection curves of the experimental results and those conforming to ACI standards. In general, the FRP design guidelines yielded precise outcomes that were consistent with the experimental results for both the traditional SCC and UFS-based GFRP SCC beams. The average deviation was just 0.90 based on ACI standards [70]. On average, the load-carrying capacities differed by less than 6 % between the conventional and UFS-based GFRP-reinforced SCC beams, underscoring the accuracy of the FRP design recommendations.

Table 7. Comparison of results between experimental and prediction

Beam	ρ_f/ρ_{fb}	Experimental		Theoretical (ACI 440-1R-15)		Exp: ACI [%]	
		P [kN]	Δ [mm]	**P** [kN]	Δ [mm]	**P** [kN]	Δ [mm]
A0-G1	0.95	59.5	32.47	60.87	30.09	-2.27	7.60
A0-G2	1.42	69.61	31.52	67.78	28.11	2.66	11.43
A30-G1	0.71	61.47	33.47	62.68	30.71	-1.94	8.60
A30-G2	1.07	73.7	33.13	70.01	30.21	5.13	9.22
Mean						**0.90**	**9.21**

Table 8. ACI design code guidelines for FRP [70]

Design of flexure		
Description	**ACI 440. 1R-15**	**Remarks**
To design tensile strength	$f_{fu} = C_E f_{fu}^*$ $\varepsilon_{fu} = C_E \varepsilon_{fu}^*$	Ensuring optimal tensile strength for FRP design
Balanced reinforcement ratio	$\rho_f = 0.85\beta_1 \frac{f'_c}{f_{fu}} \frac{\varepsilon_{cu} E_f}{\varepsilon_{cu} E_f + f_{fu}}$	The ratio provides an optimal balance between tensile reinforcement and concrete strength for reinforced concrete members
Stress block parameters	$\beta_1 = \left(0.85 - 0.05\left(\frac{f'_c - 28}{7}\right)\right) \geq 0.65$	Influencing structural behaviour and design accuracy in concrete analysis
FRP reinforcement ratio	$\rho_f = \frac{A_f}{bd}$	When $\rho_f > 1.4\ \rho_{fb}$, the design is over reinforced section When $\rho_f < \rho_{fb}$, the section is under-reinforced When $\rho_{fb} \leq \rho_f \leq 1.4\rho_{fb}$, the section was considered to be balanced reinforced
Nominal moment capacity	$M_n = \rho_f f_f \left(1 - 0.59 \frac{\rho_f f_f}{f'_c}\right) bd^2$ $f_f = \sqrt{\frac{(E_f \varepsilon_{cu})^2}{4} + \frac{0.85\beta_1 f'_c}{\rho_f} E_f \varepsilon_{cu}} - 0.5 E_f \varepsilon_{cu} \leq f_{fu}$	For the reinforced section, where f_f - stress in the FRP reinforcement in tension and must be less than or equal to the ultimate tensile strength of the FRP reinforcement (f_{fu})
	$M_n = A_f f_{fu} \left(d - \frac{\beta_1 c_b}{2}\right)$ $c_b = \frac{\varepsilon_{cu}}{\varepsilon_{cu} + \varepsilon_f} \cdot d$	For an under-reinforced section, ACI provides a traditional and simple method for obtaining the nominal flexural capacity, and it must be $M_n \geq M_u/\phi$
Calculation of midspan deflection		
Effective moment of inertia	$I_e = \frac{I_{cr}}{1 - \gamma\left(\frac{M_{cr}}{M_a}\right)^2 \left[1 - \frac{I_{cr}}{I_g}\right]} \leq I_g$	Used to calculate the midspan deflection

Table 8. ACI design code guidelines for FRP [70]

Calculation of midspan deflection		
Description	**ACI 440. 1R-15**	**Remarks**
Factor γ	$\gamma = 1.72 - 0.72\frac{M_{cr}}{M_a}$	It is influenced by the load and boundary conditions, and it accounts for the length of the uncracked portions of the member as well as the change in stiffness in the cracked areas of the FRP-RC beam
Cracking moment	$M_{cr} = \frac{\left(1.24 I_g \sqrt{f'_c}\right)}{h}$	The cracking moment is smaller than or equal to applied moment, i.e. $M_{cr} \leq M_a$
Gross moment of inertia	$I_g = \frac{bd^3}{12}$	The gross moment of inertia is greater than or equal to moment of inertia, i.e. $I_e \leq I_g$
Moment of inertia	$I_{cr} = \frac{bd^3}{3}k^3 + n_f A_f d^2 (1-k)^2$	To calculate the Moment of inertia of the transformed cracked section
Ratio k	$k = \sqrt{2\rho_f n_f + (\rho_f n_f)^2} - \rho_f n_f$	Ratio of the depth of neutral axis to reinforcement depth
Ratio n_f	$n_f = \frac{E_f}{E_c}$	Ratio of modulus of elasticity of FRP bars to the modulus of elasticity of concrete

4. Conclusion

This study analysed 12 GFRP-reinforced beams split into two groups: six used traditional SCC and six used UFS-based SCC (with 30 % UFS content). The objective was to evaluate their performance under two-point loading. The investigation included load-deformation relationship analysis, flexural design based on ACI guidelines, and a comparison of experimental results with ACI predictions. Based on the combined findings of the experimental and analytical investigations, the following conclusions were drawn.

- Under-reinforced beams fail because of GFRP rupture, whereas balanced reinforcement leads to combined bar rupture and concrete crushing failures. Over-reinforced beams mainly failed due to concrete crushing in the compression zone.
- Theoretical ACI predictions consistently overestimated (= 0.68) and underestimated (= 1.03) load values for GFRP-reinforced beams.
- Increasing the reinforcement ratio from 0.68 % to 1.03 % in the SCC beams enhanced the load-carrying capacity and reduced the midspan deflection. The concrete strength minimally affected the parameters, with SCCA30 slightly outperforming SCC A0.
- The under-reinforced beams experienced strains near the ultimate strain in the reinforcement, indicating tension failure. The balanced beams exhibited strains approaching the ultimate levels in both the reinforcement and concrete, indicating a balanced failure. Over-reinforced beams approached the ultimate concrete strain but not the reinforcement strain, signifying compression failure.
- The optimal combination was observed in SCC with 30 % UFS replacement of cement paired with GFRP reinforcement. A comprehensive exploration of the flexural behaviour of this composite system requires further experiments and numerical simulations.

Nomenclature

a - Shear span length
A_f - Area of FRP reinforcement
b - Width of rectangular cross-section
c - Distance from extreme compression fibre to the neutral axis
c_b - Distance from extreme compression fibre to the neutral axis at balanced strain condition
c_E - Environmental reduction factor
d - Effective depth of the beam
E_c - Modulus of elasticity of concrete
E_f - Modulus of elasticity of FRP
f'_c - Specified compressive strength of concrete
f_f - Stress in FRP reinforcement in tension
f_{fu} - Design tensile strength of FRP
f_{fu}^* - Guaranteed tensile strength of FRP
I_{cr} - Moment of inertia of transformed cracked section
I_e - Effective moment of inertia
I_g - Gross moment of inertia
k - Ratio of depth of neutral axis to reinforcement depth
L - Length

Nomenclature

M_a - Maximum service load moment
M_{cr} - Cracking moment
M_n - Nominal moment capacity
M_u - Factored moment at section
n_f - Ratio of modulus of elasticity of FRP bars to modulus of elasticity of concrete
P - Load
β - Stress block parameter
Δ - Mid-span deflection
ε_c - Strain in concrete
ε_{cu} - Ultimate strain in concrete
ε_f - Strain in FRP reinforcement
ε_{fu} - Design rupture strain of FRP reinforcement
ε_{fu}^* - Guaranteed rupture strain of FRP reinforcement
ϕ - Strength reduction factor
γ - Factor influenced by the load and boundary conditions
ρ_f - FRP reinforcement ratio
ρ_{fb} - FRP balanced reinforcement ratio

REFERENCES

[1] Dai, L., Bian, H., Wang, L., Potier-Ferry, M., Zhang, J.: Prestress loss diagnostics in pretensioned concrete structures with corrosive cracking, J. Struct. Eng., 146 (2020) 3, doi: 10.1061/(asce)st.1943-541x.0002554.

[2] Wang, L., Dai, L., Bian, H., Ma, Y., Zhang, J.: Concrete cracking prediction under combined prestress and strand corrosion, Struct. Infrastruct. Eng., 15 (2019) 3, pp. 285–295, doi: 10.1080/15732479.2018.1550519.

[3] Sun, Z.Y., Yang, Y., Qin, W.H., Ren, S.T., Wu, G.: Experimental study on flexural behavior of concrete beams reinforced by steel-fiber reinforced polymer composite bars, J. Reinf. Plast. Compos., 31 (2012) 24, pp. 1737–1745, doi: 10.1177/0731684412456446.

[4] Saleh, Z., Goldston, M., Remennikov, A.M., Sheikh, M.N.: Flexural design of GFRP bar reinforced concrete beams: An appraisal of code recommendations, J. Build. Eng., 25 (2019) 3, p. 100794, doi: 10.1016/j.jobe.2019.100794.

[5] Ascione, L., Mancusi, G., Spadea, S.: Flexural behaviour of concrete beams reinforced with GFRP bars, Strain, 46 (2010) 5, pp. 460–469, doi: 10.1111/j.1475-1305.2009.00662.x.

[6] Roja, S.Y., Gandhi, P., Pukazhendhi, D., Elangovan, R.: Studies on flexural behavior of concrete beams reinforced with GFRP bars, Int. J. Sci. Eng. Res., 5 (2014) 6, pp. 82–90, doi: 10.5762/kais.2014.15.8.5318.

[7] Zemour, N., Asadian, A., Ahmed, E.A., Khayat, K.H., Benmokrane, B.: Experimental study on the bond behavior of GFRP bars in normal and self-consolidating concrete, Constr. Build. Mater., 189 (2018), pp. 869–881, doi: 10.1016/j.conbuildmat.2018.09.045.

[8] Mehany, S., Mohamed, H.M., Benmokrane, B.: Contribution of lightweight self-consolidated concrete (LWSCC) to shear strength of beams reinforced with basalt FRP bars, Eng. Struct., 231 (2021) 8, doi: 10.1016/j.engstruct.2020.111758.

[9] Mehany, S., Mohamed, H.M., El-Safty, A., Benmokrane, B.: Bond-dependent coefficient and cracking behavior of lightweight self-consolidating concrete (LWSCC) beams reinforced with glass- and basalt-FRP bars, Constr. Build. Mater., 329 (2022) 4, p. 127130, doi: 10.1016/j.conbuildmat.2022.127130.

[10] Jagadeesan, S., Kumaran, G.: Struct and tie model for the analysis of RC beam-column joints reinforced woth non-metallic reinforcements, Journal of Structural Engineering India, 39 (2012) 1, pp. 140–145

[11] Saravanan, J., Kumaran, G.: Joint shear strength of exterior beam-column joints reinforced with non-metallic reinforcements, Int. J. Struct. Eng., 3 (2012) 3, pp. 137–159, doi: 10.1504/IJSTRUCTE.2012.047708.

[12] Golafshani, E.M., Rahai, A., Sebt, M.H.: Bond behavior of steel and GFRP bars in self-compacting concrete, Constr. Build. Mater., 61 (2014), pp. 230–240, doi: 10.1016/j.conbuildmat.2014.02.021.

[13] Goldston, M.W., Remennikov, A., Sheikh, M.N.: Flexural behaviour of GFRP reinforced high strength and ultrahigh strength concrete beams, Constr. Build. Mater., 131 (2017), pp. 606–617, doi: 10.1016/j.conbuildmat.2016.11.094.

[14] Goldston, M., Remennikov, A., Sheikh, M.N.: Experimental investigation of the behaviour of concrete beams reinforced with GFRP bars under static and impact loading, Eng. Struct., 113 (2016), pp. 220–232, doi: 10.1016/j.engstruct.2016.01.044.

[15] Uğur, A.E., Ünal, A.: Assessing the structural behavior of reinforced concrete beams produced with macro synthetic fiber reinforced self-compacting concrete, Structures, 38 (2022), pp. 1226–1243, doi: 10.1016/j.istruc.2022.02.051.

[16] Sashidhar, C., Jawahar, J.G., Kavyateja, B.V.: Structural behaviour of reinforced self-compacting concrete incorporating Alccofine and fly ash, J. Civ. Eng. Inter. Discip., 2 (2021) 1, pp. 10–16, 2021

[17] Kavyateja, B.V., Guru Jawahar, J., Sashidhar, C.: Effectiveness of Alccofine and fly ash on mechanical properties of ternary blended self-compacting concrete, Mater. Today. Proc., 33 (2020), pp. 73–79, doi: 10.1016/j.matpr.2020.03.152.

[18] Okamura, H., Ouchi, M.: Sel-Compacting Concrete, J. Adv. Concr. Technol., 1 (2003) 1, pp. 5–15

[19] Ghoddousi, P., Salehi, A.M.: Effect of mix proportion on robustness of self-compacting concrete, Građevinar, 67 (2015) 1, pp. 1–9, doi: 10.14256/JCE.1136.2014.

[20] Chidambaram, P., Jagadeesan, S.: Characteristics of self-compacting concrete with different size of coarse aggregates and Alccofine, Trends Sci., 19 (2022) 5, doi: 10.48048/tis.2022.3042.

[21] Prithiviraj, C., Swaminathan, P., Kumar, D.R., Murali, G., Vatin, N.I.: Fresh and hardened properties of self-compacting concrete comprising a copper slag, Buildings, 12 (2022) 7, doi: 10.3390/buildings12070965.

[22] Dinakar, P.: Design of self-compacting concrete with fly ash, Mag. Concr. Res., 64 (2012) 5, pp. 401–409, doi: 10.1680/macr.10.00167.

[23] Dinakar, P., Sethy, K.P., Sahoo, U.C.: Design of self-compacting concrete with ground granulated blast furnace slag, Mater. Des., 43 (2013), pp. 161–169, doi: 10.1016/j.matdes.2012.06.049.

[24] EFNARC: The European Guidelines for selfcompacting concrete, Eur. Guidel. Self-compact. Concr., http://www.efnarc.org/pdf/SCCGuidelinesMay2005.pdf, [2.5.2023.]

[25] ISO 1920-13: Testing of concrete — Part 13: Properties of fresh self-compacting concrete, Int. Stand. Organ., https://www.iso.org/standard/69414.html, [2.5.2023.]

[26] Mazloom, M., Ranjbar, A.: Relation between the workability and strength of self-compacting concrete relation between the workability and strength of self-compacting concrete, Proceedings of the 35th Conference on Our World in Concrete & Structures, Singapore, 2010.

[27] Khatri, R.P., Sirivivatnanon, V.: Effect of different supplementary cementitious materials on mechanical properties of high - performance concrete, Cem. Concr. Res., 25 (1995) 1, pp. 209–220

[28] Srinath, B.L.N.S., Patnaikuni, C.K., Balaji, K.V.G.D., Kumar, B.S., Manjunatha, M.: A prospective review of Alccofine as supplementary cementitious material, Mater. Today. Proc., 47 (2021), pp. 3953–3959, doi: 10.1016/j.matpr.2021.03.719.

[29] Boobalan, S.C., Srivatsav, V.A., Nisath, A.M.T., Babu, A.P., Gayathri, V.: A comprehensive review on strength properties for making Alccofine based high performance concrete, Mater. Today. Proc., 45 (2021), pp. 4810–4812, doi: 10.1016/j.matpr.2021.01.278.

[30] Kanellopoulos, A., Petrou, M.F., Ioannou, I.: Durability performance of self-compacting concrete, Constr. Build. Mater., 37 (2021), pp. 320–325, doi: 10.1016/j.conbuildmat.2012.07.049.

[31] Sethy, K., Pasla, D., Sahoo, U.C.: Effect of slag on the rheological and strength properties of self-compacting concrete, Key Eng. Mater., 629 (2015), pp. 399–404, doi: 10.4028/www.scientific.net/KEM.629-630.399.

[32] Narender Reddy, A., Meena, T.: A study on compressive behavior of ternary blended concrete incorporating Alccofine, Mater. Today. Proc., 5 (2018) 5, pp. 11356–11363, doi: 10.1016/j.matpr.2018.02.102.

[33] Ahmad, S., Umar, A., Masood, A., Nayeem, M.: Performance of self-compacting concrete at room and after elevated temperature incorporating Silica fume, Adv. Concr. Constr., 7 (2019) 1, pp. 31–37, doi: 10.12989/acc.2019.7.1.031.

[34] Balamuralikrishnan, R., Saravanan, J.: Effect of Alccofine and GGBS addition on the durability of concrete, Civ. Eng. J., 5 (2019) 6, pp. 1273–1288, doi: 10.28991/cej-2019-03091331.

[35] Raja Rajeshwari, B., Sivakumar, M.V.N.: Influence of coarse aggregate properties on specific fracture energy of steel fiber reinforced self-compacting concrete, Adv. Concr. Constr., 9 (2020) 2, pp. 173–181, doi: 10.12989/acc.2020.9.2.173.

[36] Schackow, A., Effting, C., Marcon Neto, D., Bonifácio, D.E., Gomes, I.R.: Properties of the self-compacting concrete with fly ashes, Rev. Eng. Civ., 57 (2020) 7, pp. 26–35

[37] Karthik, D., Nirmalkumar, K., Priyadharshini, R.: Characteristic assessment of self-compacting concrete with supplementary cementitious materials, Constr. Build. Mater., 297 (2021), p. 123845, doi: 10.1016/j.conbuildmat.2021.123845.

[38] Marinković, S., Protić, M., Paunović, S., Nešović, I., Bijeljić, J.: Application of industrial by-products as mineral admixtures for self-compacting concrete, Građevinar, 70 (2018) 1, pp. 31–38, doi: 10.14256/JCE.1516.2015.

[39] Balamuralikrishnan, R., Saravanan, J.: Effect of addition of Alccofine on the compressive strength of cement mortar cubes, Emerg. Sci. J., 5 (2021) 2, pp. 155–170, doi: 10.28991/esj-2021-01265.

[40] Srinivas, K., Sankar, L.P., Swamy, C.K.: Experimental investigation on rapid strength gain by adding Alccofine in high strength concrete, Mater. Today. Proc., 46 (2021), pp. 925–929, doi: 10.1016/j.matpr.2021.01.068.

[41] Parveen, S., Lim, Y.Y., Pham, T.M.: Effective utilisation of ultrafine slag to improve mechanical and durability properties of recycled aggregates geopolymer concrete, Clean. Eng. Technol., 5 (2021) 11, p. 100330, doi: 10.1016/j.clet.2021.100330.

[42] Sagar, B., Sivakumar, M.V.N.: An experimental and analytical study on Alccofine based high strength concrete, Int. J. Eng. Trans. A Basics, 33 (2020) 4, pp. 530–538, doi: 10.5829/IJE.2020.33.04A.03.

[43] Reddy, P.N., Jindal, B.B., Kavyateja, B.V., Narender Reddy, A.: Strength enhancement of concrete incorporating Alccofine and SNF based admixture, Adv. Concr. Constr., 9 (2020) 4, pp. 345–354, doi: 10.12989/acc.2020.9.4.345.

[44] Prithiviraj, C., Saravanan, J.: Influence of W/B ratio and chemical admixture on fresh and hardened properties of self-compacting concrete using Alccofine, J. Xidian Univ., 14 (2020) 5, pp. 4906–4915, doi: 10.37896/jxu14.5/537.

[45] Kavyateja, B.V., Jawahar, J.G., Sashidhara, C.: Durability performance of self-compacting concrete incorporating Alccofine and fly ash, Int. J. Eng. Trans. B Appl., 33 (2020) 8, pp. 1522–1528, doi: 10.5829/ije.2020.33.08b.10.

[46] Prithiviraj, C., Saravanan, J., Kumar, D.R., Murali, G., Vatin, N.I., Swaminathan, P.: Assessment of strength and durability properties of self-compacting concrete comprising Alccofine, Sustain., 14 (2022) 10, p. 5895, doi: 10.3390/su14105895.

[47] Sagar, B., Sivakumar, M.V.N.: Mechanical and microstructure characterization of Alccofine based high strength concrete, Silicon, 14 (2022) 3, pp. 795–813, doi: 10.1007/s12633-020-00863-x.

[48] Saloni, A., Singh, V., Sandhu, A., Jatin, I., Parveen, J.: Effects of Alccofine and curing conditions on properties of low calcium fly ash-based geopolymer concrete, Mater. Today. Proc., 32 (2020), pp. 620–625, doi: 10.1016/j.matpr.2020.02.763.

[49] Vivek, K.C., Palanisamy, M., Debnath, S., Munagala, M.: Performance evaluation of durability and flexural behaviour of self-compacting concrete blended with Alccofine, IOP Conf. Ser. Mater. Sci. Eng.,1126 (2021) 1, p. 012083, doi: 10.1088/1757-899x/1126/1/012083.

[50] Prithiviraj, C., Saravanan, J.: Flexural performance of Alccofine-based self-compacting concrete reinforced with steel and GFRP bars, Int. Trans. J. Eng. Manag. Appl. Sci. Technol., 12 (2021) 8, pp. 1–12, doi: 10.14456/ITJEMAST.2021.168.

[51] Nanni,A.: Flexural behavior and design of RC members using FRP reinforcement, J. Struct. Eng., 119 (1993) 11, pp. 916–917, doi: 10.1061/(asce)0733-9445(1995)121:5(916.2).

[52] Benmokrane, B., Chaallal, O., Masmoudi, R.: Glass fibre reinforced plastic (GFRP) rebars for concrete structures, Constr. Build. Mater., 9 (1995) 6, pp. 353–364, doi: 10.1016/0950-0618(95)00048-8.

[53] Ganga Rao, P.V., Vijay, H.V.S.: Design of Concrete Members Reinforced with GFRP Bars, Proceedings of the Third International Symposium on Non-Metallic (FRP) Reinforcement for Concrete Structures (FRPRCS-3), 1997.

[54] Xiao-jie, L., Zhi-wu, Y., Li-zhong, J.: Long term behavior of self-compacting reinforced concrete beams, J. Cent. South Univ., 15 (2008) 3, pp. 423–428, doi: 10.1007/s11771.

[55] Kalpana, V.G., Subramanian, K.: Behavior of concrete beams reinforced with GFRP bars, J. Reinf. Plast. Compos., 30 (2011) 23, pp. 1915–1922, doi: 10.1177/0731684411431119.

[56] You, Z., Chen, X., Dong, S.: Ductility and strength of hybrid fiber reinforced self-consolidating concrete beam with low reinforcement ratios, Syst. Eng. Procedia, 1 (2011), pp. 28–34, doi: 10.1016/j.sepro.2011.08.006.

[57] Mazaheripour, H., Barros, J.A.O., Soltanzadeh, F., Sena-Cruz, J.: Deflection and cracking behavior of SFRSCC beams reinforced with hybrid prestressed GFRP and steel reinforcements, Eng. Struct., 125 (2016), pp. 546–565, doi: 10.1016/j.engstruct.2016.07.026.

[58] Nikbin, I.M., Davoodi, M.R., Fallahnejad, H., Rahimi, S., Farahbod, F.: Influence of mineral powder content on the fracture behaviors and ductility of self-compacting concrete, J. Mater. Civ. Eng., 28 (2016) 3, pp. 1–14, doi: 10.1061/(asce)mt.1943-5533.0001404.

[59] Koya, B., Sureshkumar, M.: High strength self-compacting concrete reinforced beams with steel and GFRP bars: Performance of fly-ash and GGBS-based materials, Eur. Chem. Bull., 12 (2023) 6, pp. 4286–4295

[60] Mithra, M., Ramanathan, P., Muthupriya, P., Venkatasubramani, R.: Flexural behavior of reinforced self-compacting concrete containing GGBFS, Int. J. Eng. Innov. Technol., 1 (2012) 4, pp. 124–129

[61] Patel, S., Balakrishna, H.B.: Flexural behaviour of reinforced concrete beams replacing GGBS as cement and slag sand as fine aggregate, Int. J. Civ. Struct. Eng. Res., 2 (2014) 1, pp. 66–75

[62] Marshaline Seles, M., Suryanarayanan, R., Vivek, S.S., Dhinakaran, G.: Study on flexural behaviour of ternary blended reinforced self-compacting concrete beam with conventional RCC beam, IOP Conference Series: Earth and Environmental Science, 80 (2017) 1, doi: 10.1088/1755-1315/80/1/012026.

[63] Manju, R., Premalatha, J., Shanthi, R., Aishwaryalakshmi, V.: Flexural behaviour of self-compacting concrete beams, Int. J. Civ. Eng. Technol., 8 (2017) 9, pp. 305–318

[64] Vivek, S.S., Narayanan, R.S., Dhinakaran, G.: Comparative study on flexural behaviour of RCC beam and SCC ternary beams with mineral admixtures, Constr. Build. Mater., 152 (2017), pp. 57–64, doi: 10.1016/j.conbuildmat.2017.06.160.

[65] Shijumon, V., Nalanth, N.: Flexural behaviour of self-compacting concrete beams modified using recycled concrete waste aggregates, Int. J. Recent Technol. Eng., 8 (2019) 2, pp. 3413–3417, doi: 10.35940/ijrte.B2296.078219.

[66] IS:12269-2013: Ordinary Portland Cement, 53 grade specification, Indian Stand., (2013) 3 pp. 1–14

[67] IS:383-2016: Specification for coarse and fine aggregates from natural sources for concrete, Indian Stand., (2016) 4, pp. 1–24

[68] IS:9103-2018: Concrete admixtures specification, Indian Stand., (2018) 4.

[69] D7205/D7205M – 06: Standard Test Method for tensile properties of fiber reinforced polymer matrix composite bars, Am. Soc. Test. Mater., (2006) 2, pp. 1–12, https://www.astm.org/d7205_d7205m-06r16.html, [10.4.2010.]

[70] ACI Committee: Guide for the design and construction of structural concrete reinforced with firber-reinforced polymer (FRP) bars (ACI440.1R-15), 22 (2015) 4.

[71] Adam, M.A., Said, M., Mahmoud, A.A., Shanour, A.S.: Analytical and experimental flexural behavior of concrete beams reinforced with glass fiber reinforced polymers bars, Constr. Build. Mater., 84 (2015), pp. 354–366, doi: 10.1016/j.conbuildmat.2015.03.057.

[72] Ashour, A.F., Habeeb, M.N.: Continuous concrete beams reinforced with CFRP bars, Proc. Inst. Civ. Eng. Struct. Build., 161 (2008) 6, pp. 349–357, doi: 10.1680/stbu.2008.161.6.349.

[73] Canadian Standards Association: Design and construction of building components with fibre-reinforced polymers (CAN/CSA S806-02), p. 177, 2009.

[74] ISIS Canada Research Network: Reinforcing concrete structures with fibre reinforced polymers, (2007) 3.

[75] Faza, S.S., Ganga Rao, H.V.S.: Theoretical and experimental correlation of behavior of concrete beams reinforced with fiber reinforced plastic rebars, American Concrete Institute Special Publication, 138 (1993), pp. 599–614, doi: 10.14359/3942.

[76] Theriaule, M., Benmokrane, B.: Effects of FRP reinforcement ratio and concrete strength, J. Compos. Constr., 2 (1998) 2, pp. 7–16